Colloid Polym Sci 279:1090–1096 (2001)

ORIGINAL CONTRIBUTION

G. Lagaly
O. Mecking
D. Penner

Colloidal magnesium aluminum hydroxide and heterocoagulation with a clay mineral. I. Properties of colloidal magnesium aluminum hydroxide

Received: 28 February 2001
Accepted: 8 March 2001

G. Lagaly (✉)
Universität Kiel
Institut für Anorganische Chemie
24098 Kiel, Germany
e-mail: h.mittag@email.uni-kiel.de

O. Mecking
Thüringisches Landesamt für
Denkmalpflege, Abteilung Archäometrie
Humboldtstrasse 11, 99443 Weimar
Germany

D. Penner
Forschungsinstitut für anorganische
Werkstoffe–Glas/Keramik–GmbH
Heinrich-Meister-Strasse
56203 Höhr-Grenzhausen, Germany

Abstract Magnesium aluminum hydroxide, the most important member of layered double hydroxides, was peptized by intense washing. The particle diameter, 70–130 nm, depended on the temperature of aging the parent material. The electrophoretic mobility of the particles decreased with increasing pH, from 3.7×10^{-8} m^2/Vs at pH 5 to 0.5×10^{-8} m^2/Vs at pH 12.3. An isoelectric point at pH $\sim$ 7 was reached with the addition of 87 mmol/l NaSCN, 3 mmol/l Na_2SO_4 and Na_2CO_3, and 0.7 mmol/l Na_2HPO_4. The critical coagulation concentration for the 2% (w/w) dispersion was 88 mmol/l NaCl, 1.8 mmol/l Na_2CO_3, 1.4 mmol/l Na_2SO_4, and 1.2 mmol/l Na_2HPO_4 at pH $\sim$ 7. The 2% dispersion at pH $\sim$ 7 showed an almost Newtonian flow behavior. Yield values were developed after salt addition. The 2% dispersion reached a yield value of 2 Pa at 100 mmol/l NaCl, 3 Pa at 100 mmol/l Na_2SO_4, and 5 Pa at 100 mmol/l Na_2CO_3. Sodium phosphate in comparison with the other salts showed a liquefying effect. The yield value increased to 3 Pa at 1–10 mmol/l Na_2HPO_4 and decreased to 0.5 Pa at 100 mmol/l Na_2HPO_4.

Key words Coagulation · Colloids · Electrophoretic mobility · Hydrotalcite · Layered double hydroxide

Introduction

Layered materials with interlamellar reactivity (ion exchange, intercalation, swelling) form a group of platelike colloidal particles with peculiar properties [1]. Widely known are clay minerals such as montmorillonites, which are the dominant components in bentonites [2–4]. Almost all layered compounds are composed of negatively charged layers separated by interlayer cations [5]. Only layered double hydroxides (sometimes called "anionic clays") consist of positively charged layers and interlayer anions. The general composition is

$$\left[M_{1-x}M_x^{\mathrm{III}}(\mathrm{OH})_2\right]^{\xi+}X_{\xi/n}^{n-} \cdot z\mathrm{H_2O}\ .$$

Usually, M is a divalent cation (Mg^{2+}, Ca^{2+}, Zn^{2+}, etc.), but can also be Li^+. M^{III} is a trivalent cation such as Al^{3+}, Cr^{3+}, Fe^{3+}, Co^{3+}. X^{n-} (Cl^-, NO_3^-, ClO_4^-, CO_3^{2-}, SO_4^{2-}, etc.) is the interlayer anion, and ξ is the layer charge ($\xi = x$ for $M = M^{\mathrm{III}}$, $\xi = 2x-1$ for $M = Li^+$). The structure is composed of layers of $M(OH)_6$ octahedra as in brucite [$Mg(OH)_2$]. The divalent and trivalent cations occupy the centers of the octahedra [6–8]. The anions together with water molecules are arranged between the layers [9]. The hydroxide layers are 0.48–0.49-nm thick, the distance between the hydroxyl groups within one layer in the c direction is 0.20 nm.

The degree of substitution is not fixed by the structure and can vary between $M^{\mathrm{II}}/M^{\mathrm{III}} = 4{:}1$ ($x = 0.2$) and $M^{\mathrm{II}}/M^{\mathrm{III}} = 3{:}2$ ($x = 0.4$). The mineral hydrotalcite (pyroaurite group) contains magnesium and aluminum ions in the molar ratio of 3:1 or 2:1 with carbonate as an interlayer anion, corresponding to $[Mg_3Al(OH)_8](CO_3)_{0.5} \cdot 2H_2O$ ($x = 0.25$) and $[Mg_2Al(OH)_6]$

$(CO_3)_{0.5} \cdot H_2O$ ($x = 0.33$) [6]. Manasseite shows the same composition, $[Mg_3Al(OH)_8](CO_3)_{0.5} \cdot 2H_2O$, but belongs to the sjögrenite group. Pyroaurite and sjögrenite differ in the type of stacking of the hydroxide layers [6].

A wide range of double hydroxides can be synthesized by coprecipitation of the two hydroxides or from gels under mild hydrothermal conditions [7, 10–22].

Anion-exchange reactions were first described by Dosch (calcium aluminum hydroxide) [23, 24], Miyata and Kumura (magnesium aluminum hydroxide) [25], Boehm et al. [10], and Kopka et al. [11] (zinc chromium hydroxide). Drezdon [26] reported the intercalation of terephthalate anions and the subsequent exchange by polyoxometalate ions such as $Mo_7O_{24}^{6-}$ and $V_{10}O_{28}^{6-}$. In the meantime, many different types of organic derivatives were prepared [27, 28].

The interest in layered double hydroxides is based on their adsorption and catalytic properties [27, 29, 30]. Most common is magnesium aluminum hydroxide, which is produced on an industrial scale. It is also used as an antacid.

The properties of colloidal layered double hydroxides are hardly known. The hydroxides crystallize easily, and it is difficult to obtain them in the colloidal state. Albiston et al. [31] prepared colloidal magnesium aluminum hydroxide with particle diameters of 60–770 nm by reacting solid MgO with aluminum nitrate solution. We obtained the colloidal fraction by peptizing magnesium aluminum hydroxide during several washing steps. In a similar way, Han et al. [32] obtained very small particles (diameter about 12 nm) of magnesium aluminum hydroxide.

Materials and methods

Magnesium aluminum hydroxide

The double hydroxide was prepared by coprecipitation of magnesium and aluminum hydroxide at alkaline pH [13, 33]. Amounts of 0.32 mol $Mg(NO_3) \cdot 6H_2O$ and 0.16 mol $Al(NO_3)_3 \cdot 9H_2O$ were dissolved in 1000 ml water. This solution was added (dropwise within 1 hour) to a solution of 1.1 mol NaOH and 0.15 mol $NaNO_3$ in 1000 ml water. A white, voluminous precipitate formed. The dispersion was aged for 6 days at 0, 20, 50, and 90 °C. At higher temperatures the dispersion turned into a rigid gel.

The aged double hydroxide was separated by centrifugation (20 min, 2000 rpm = 380*g*, Heraeus Biofuge). The hydroxide settled completely. The sediment was redispersed in 800 ml water (Ultra Turrax). After centrifugation a small amount of the hydroxide remained dispersed. The sedimentation/redispersion procedure was repeated several times. The turbid supernatents were collected (solid content about 1%). The number of sedimentation/redispersion steps was strongly reduced when the aged material was dialyzed for 2 or more weeks until the conductivity of the water was below 10 μS/cm. Dried powders were obtained by freeze-drying or spray-drying. The materials extracted from the samples aged at 0, 20 °C, etc. were designated as MAH-0, MAH-20, etc.

The pH value of the dispersions varied between 11.5–12.5 and decreased to 9 during the sedimentation/redispersion procedure. The dispersion aged at 50 °C did not peptize. In this case the pH decreased to 7 during the washing cycles. The sediment was not repeptized after addition of NaOH.

The freeze-dried and the spray-dried samples could easily be dispersed in water. Colloidal dispersions (2% w/w solid content) were prepared by stirring the freeze-dried or spray-dried material in water for 24 h. The pH of these dispersions was about 7.

Chemical analysis

We measured the magnesium and aluminum contents of the dispersion with an atom emission spectrometer (Spectraspan IV, Beckman Instruments). The water content was determined by thermogravimetric analysis. To measure the adsorption of inorganic anions by ion exchange and the numbers of displaced nitrate ions, volumes of 1 ml salt solutions of different concentrations were added to 1 ml of the 2% (w/w) magnesium aluminum hydroxide dispersion. After shaking the samples overnight, the solid material was separated by centrifugation. The concentration of the salts in the solution was determined by ion chromatography (high-pressure liquid chromatography, Waters [34]).

Particle size

The particle size (Stokes equivalent diameter, d_S) was determined by sedimentation (cuvette photocentrifuge, Horiba Capa 500). The density needed for evaluating the data was 2.23 g/cm^3 (helium pressure measurement of freeze-dried samples). The mean equivalent spherical diameter, d_R, was measured by dynamic light scattering (ZetaPlus, Brookhaven Instruments). The relation d_R/d_S indicates the axial ratio of the particles [35].

Electrophoretic mobility and colloidal stability

The electrophoretic mobility of the hydroxide particles was measured by microelectrophoresis (PenKem 501). The critical coagulation concentration was obtained by test-tube tests [1, 36]. An amount of 1 ml hydroxide dispersion (2% w/w solid content) was added to 1 ml salt solution. The tubes were turned ten times. After resting for 24 h, the colloidal state of the dispersion (stable sol or coagulated) was determined by visual inspection.

Rheological measurements

The flow behavior was measured using a Physica UDS 200 rotational viscometer with cone–plate geometry (plate diameter 5 cm, distance 0.05 cm) [37]. The dispersion was first sheared at a rate of $\dot{\gamma} = 50/s$ for 1 min, then remained at rest for a further minute before the shear rate/shear stress curves were recorded between 0 and 2000/s. The yield value was obtained by extrapolating the linear section of the curve at the highest shear rates to $\dot{\gamma} = 0$.

The storage (G') and loss (G'') moduli were determined by oscillating measurements (deformation 1%, frequency 3.5 Hz). The dispersion was sheared at $\dot{\gamma} = 50/s$ within 1 min, then allowed to rest for 2 min before the oscillation measurements were started. Linear viscoelastic behavior was observed up to a frequency of 10 Hz at a deformation of 1% [37].

Results

Analytical composition

The starting material (MAH-20) had a Mg^{2+}/Al^{3+} molar ratio of 2.57 corresponding to $[Mg_{2.16}Al_{0.84}(OH)_6]^{0.84+}$ ($x = 0.28$). The water content (by

thermogravimetric analysis) was 1 mol H_2O per mole $[Mg_{2.16}Al_{0.84}(OH)_6]^{0.84+}$. The interlayer space contained about 60 mol% nitrate, about 5 mol% chloride, and about 35 mol% carbonate. Carbonate ions are tightly bound in the interlayer space [38]. Without strong protection against CO_2, preparation of the nitrate form always yields products with interlayer carbonate anions. It seems that the transformation of solid MgO with aluminum chloride solutions [31] into the double hydroxide reduced the amount of carbonate because of the lower pH value. Equilibration with salt solutions revealed that the carbonate ions were not exchanged by chloride, sulfate, and phosphate.

The colloidal samples extracted by peptizing the parent material showed Mg^{2+}/Al^{3+} molar ratios of about 1.9 ($x \sim 0.34$). For instance, the previously described material yielded colloidal fractions with Mg^{2+}/Al^{3+} ratios of 1.95, 1.83, and 1.88 after washing steps 4, 5, and 6.

Particle shape and size

The colloidal magnesium aluminum hydroxide consisted of platelets of irregular shape. The particles obtained by the different washing steps showed similar size and size distributions. The size depended on the temperature of aging (Fig. 1a, Table 1). The mean equivalent diameter (from sedimentation) was 110 nm (MAH-0), 70 nm (MAH-20), and 130 nm (MAH-90). As noted earlier, colloidal particles could not be extracted from the material aged at 50 °C. Spray-drying caused some agglomeration. The particles from the 20 °C material revealed a similar size distribution below 200 nm as the nondried sample but the other samples showed a pronounced depletion of finer particles (Fig. 1b). The reason is that the spray-drying conditions were optimized for the 20 °C sample. In other words: the particle size distribution changed when the conditions of spray-drying were not optimal.

Critical coagulation concentration

The three samples of colloidal hydroxides had similar critical coagulation concentrations. The 90 °C sample

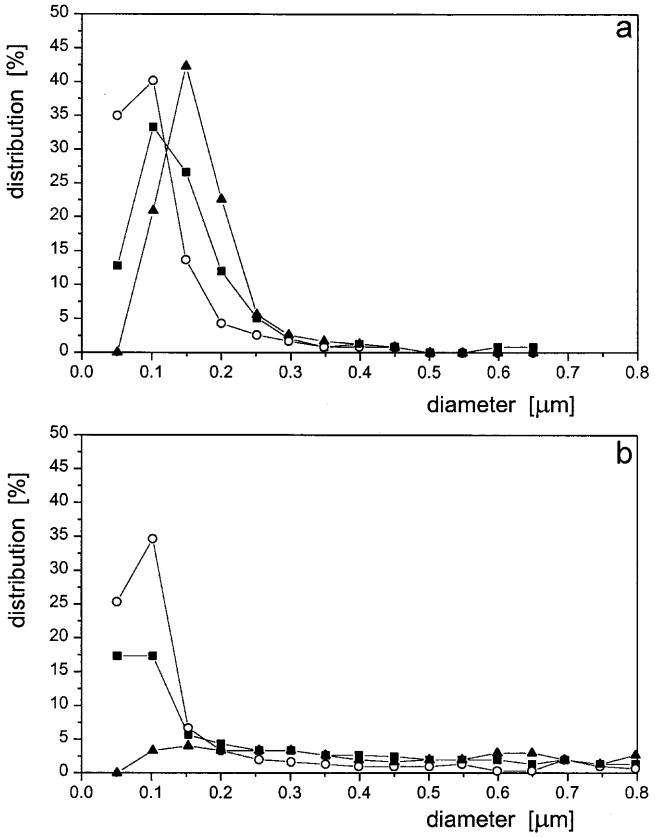

Fig. 1 Particle size distribution of colloidal magnesium aluminum hydroxides. The parent material was altered at 0 °C (■), 20 °C (○), and 90 °C (▲): **a** colloid fractions obtained by washing steps 4–6; **b** as **a** after spray-drying and redispersion

was slightly less stable than MAH-0 and MAH-20 (Tables 1, 2). Monovalent counterions coagulated at concentrations of 60–88 mmol/l (Tables 2, 3). Divalent anions showed c_K values of 1–1.8 mmol/l (Table 2). Long-term dialysis of the material aged at 20 °C instead of several washing steps yielded a colloidal dispersion with sligthly smaller c_K values (50 mmol/l NaCl, 35 mmol/l $NaNO_3$ for the 0.2% dispersion). Preparation of the hydroxide in the absence of CO_2 did not distinctly influence the critical coagulation concentrations

Table 1 Mean particle size (cuvette photocentrifuge), mobility, and critical coagulation concentration of colloidal magnesium aluminum hydroxide from parent materials aged at 0 °C (MAH-0), 20 °C (MAH-20), and 90 °C (MAH-90)

	MAH-0	MAH-20	MAH-90
Particle diameter (nm)	110	70	130
Mobility (m^2/Vs)[a]	2.7×10^{-8}	2.8×10^{-8}	2.2×10^{-8}
Critical coagulation concentration (mmol/l)[b]			
NaCl	86	88	66
Na_2SO_4	1.4	1.4	1.3
Na_2HPO_4	1.2	1.2	1

[a] Spray-dried and redispersed, solid content 0.06%, pH ~ 7
[b] Spray-dried and redispersed, solid content 1% w/w, pH ~ 7

Table 2 Critical coagulation concentration of sodium salts. 1% (w/w) hydroxide dispersion (MAH-20, spray-dried and redispersed)

Salt	c_K (mmol/L)	Salt	c_K (mmol/l)
NaCl	88	Na_2CO_3	1.8
NaBr	86	Na_2SO_4	1.4
NaSCN	80	Na_2HPO_4	1.2

Table 3 Critical coagulation concentration (NaCl) of hydroxide dispersions, solid content about 0.2% (w/w). The parent materials were prepared at different Mg^{2+}/Al^{3+} molar ratios, $NaNO_3$ and NaOH contents

Mg^{2+}/Al^{3+}	NaOH/Al^{3+} (mol/mol)	$NaNO_3$/Al^{3+} (mol/mol)	c_K (mmol/l)
5	14.1	1.92	30
2[a]	7.1	0.96	61[b]
1	4.7	0.64	9
0.5	3.5	0.48	7
0.1	2.8	0.39	3
2	7.1	0.38	30
2	7.1	0.77	50
2[a]	7.1	0.96	61
2	7.1	1.15	60
2	7.1	1.54	60
2	4.8	0.96	9
2[a]	7.1	0.96	61
2	8.0	0.96	50
2	11.2	0.96	60

[a] Corresponding to MAH–20
[b] c_K of $NaNO_3$: 70 mmol/l

(50 mmol/l NaCl, 70 mmol/l $NaNO_3$, 0.2% dispersion) because the carbonate anions of the otherwise prepared samples were mainly bound in the interlayer space.

An interesting observation was that the critical coagulation concentration depended on the magnesium/aluminum ratio. The maximum value was observed when this ratio was 2. At Mg/Al ratios different from 2, the c_K value (NaCl) was distinctly smaller (Table 3). The c_K value also decreased at low $NaNO_3$ and NaOH contents (Table 3).

Electrophoretic mobility

The mobility of the hydroxide particles was strongly pH dependent. It decreased from $\mu = 3.7 \times 10^{-8}$ m^2/Vs at pH 5, reached some kind of a plateau at pH $\sim$ 6.5–8.5 ($\mu = 2.8 \times 10^{-8}$ m^2/Vs), and decreased to 0.5×10^{-8} m^2/Vs at pH 12.3 (Fig. 2). It was independent of the concentration of NaCl, NaBr, NaI, and $NaNO_3$ but decreased in the presence of NaSCN ($\mu = -0.8 \times 10^{-8}$ m^2/Vs at 100 mmol/l NaSCN). The isoelectric point was reached at 87 mmol/l NaSCN (Fig. 3a).

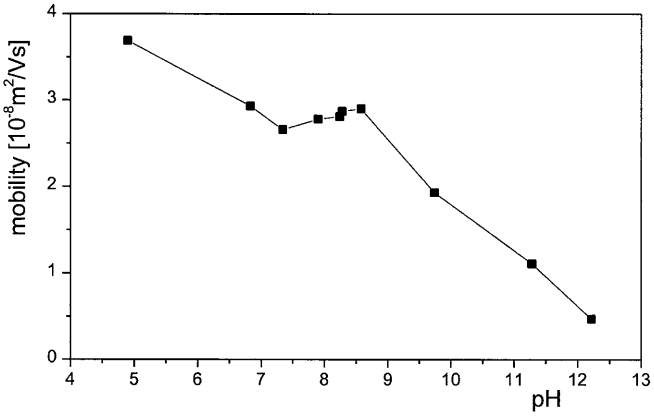

Fig. 2 Mobility of the hydroxide particles (sample MAH-20) as a function of solution pH

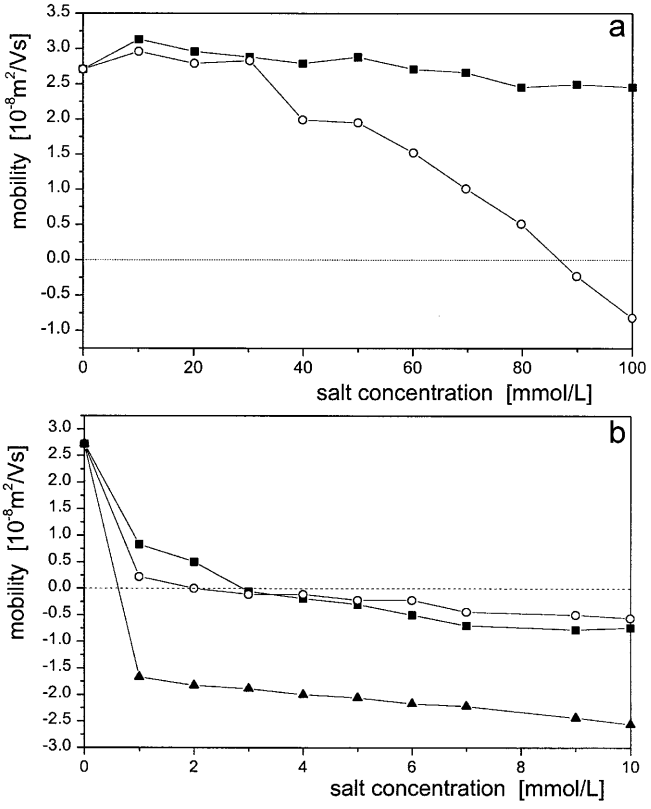

Fig. 3 Mobility of the hydroxide particles (sample MAH-20) at pH $\sim$ 7 and different salt concentrations: **a** NaCl (■), NaSCN (○); **b** Na_2SO_4 (■), Na_2CO_3 (○), Na_2HPO_4 (▲)

Divalent anions (SO_4^{2-}, CO_3^{2-}, HPO_4^{2-}) reduced the mobility very sharply (Fig. 3b). The isoelectric point was reached at extremely low salt concentrations: at 3 mmol/l Na_2SO_4 or Na_2CO_3 and 0.7 mmol/l Na_2HPO_4. The mobility increased only slightly at salt concentrations beyond 10 mmol/l and approximated, at 100 mmol/l,

-1.8×10^{-8} m^2/Vs (Na_2SO_4), -2.0×10^{-8} m^2/Vs (Na_2CO_3), and -3.6×10^{-8} m^2/Vs (Na_2HPO_4). Aging the parent material at 90 °C slightly reduced the mobility of the particles (Table 1).

Flow behavior

The 2% magnesium aluminum hydroxide dispersion showed an almost Newtonian behavior. Addition of NaCl and NaBr created a yield value which increased from about 0.3 Pa at 0.1 mmol/l to 1.9 Pa at 90 mmol/l NaCl and NaBr (Fig. 4a). The dispersions behaved slightly antithixotropically. The viscosity of the 2% dispersions increased from about 1.8 to about 2.1 mPas. Addition of NaSCN raised the yield value to 3 Pa at 100 mmol/l and produced a maximum of 2.2 Pa at 10 mmol/l. At this NaSCN concentration, the dispersion was strongly antithixotropic, but hysteresis decreased at higher salt concentrations. The viscosity showed a maximum of 2.3 mPas at 20–30 mmol/l NaSCN and decreased to 2 mPas at 100 mmol/l.

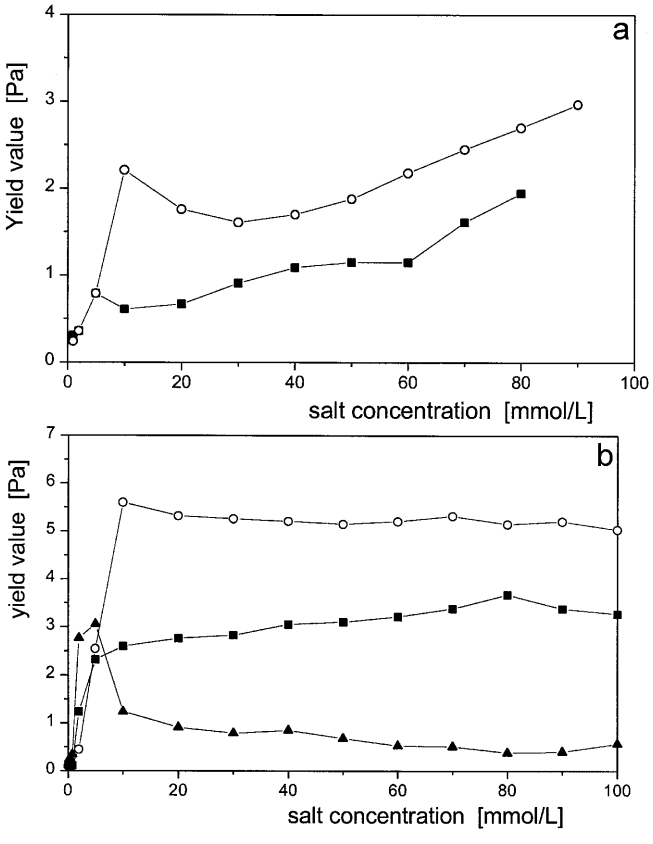

Fig. 4 Yield value of the 2% hydroxide dispersion (sample MAH-20) at pH ~ 7 in the presence of salts: **a** NaCl (very similar NaBr) (■), NaSCN (○); **b** Na_2SO_4 (■), Na_2CO_3 (○), Na_2HPO_4 (▲)

Addition of Na_2SO_4 and Na_2CO_3 increased the yield value of the 2% dispersion to 3 and 5 Pa, respectively (Fig. 4b). Amounts of 1–10 mmol/l Na_2HPO_4 increased the yield value to a maximum of about 3 Pa. Higher concentrations reduced it to 0.5 Pa (Fig. 4b). The antithixotropic behavior increased slightly with the concentration of Na_2SO_4 and Na_2CO_3. It showed a maximum around 5 mmol/l Na_2HPO_4 and disappeared beyond 50 mmol/l Na_2HPO_4. The viscosity changed in a similar way as the yield value and reached 2.7 mPas at 100 mmol/l Na_2SO_4, 3.3 mPas at 100 mmol/l Na_2CO_3, and a maximum of 2.5 mPas at 2–5 mmol/l Na_2HPO_4. It decreased to 1.7 mPas at 100 mmol/l Na_2HPO_4.

Discussion

The particle size of the peptized magnesium aluminum hydroxide seems to depend in a complicated manner on the temperature and the period of aging the parent material. These processes will be studied in more detail. Increasing temperature accelerates nucleation, particle growth, and coalescence of primary particles to larger particles but reduces the aggregation to networks. The particle size decreases from MAH-0 to MAH-20 because the increased nucleation of new particles reduces the average particle size. Aggregation during aging at 50 °C impedes peptization of the hydroxide. At still higher temperatures aggregation is reduced, and particles of larger size are formed, probably by coalescence [1].

Intense washing of the crystalline magnesium aluminum hydroxide removes excess salts, which is a basic requirement for peptization. In addition, cementing materials between the particles may be dissolved. However, washing reduced the crystallinity of the particles. The X-ray powder diagram in comparison with that of the coarse parent material showed broadened reflections. Also, the composition of the colloidal material (degree of substitution $x = 0.34$) was different from that of the starting material ($x = 0.28$). When hydroxides were prepared using different ratios of magnesium and aluminum salt solutions, the colloidal material with the Mg^{2+}/Al^{3+} ratio of about 2 showed the highest salt stability (Table 3).

Interlayer carbonate anions seem to impede the extensive decomposition of the particles during peptization. These anions hold together the hydroxide layers very tightly and are difficult to exchange by other inorganic anions [38].

The critical coagulation concentration of monovalent anions (Tables 1, 2) is typical of electrostatic stabilization and increased with the solid content (Table 3). Such an increase is observed when the coagulating counterions are strongly adsorbed [36, 39]. Specific adsorption of

chloride ions is also evident from the charge titration curves at different NaCl concentrations as reported by Han et al. [32]. The occurrence of a common intersection point different from the position of the point of zero charge is typical of specific adsorption [1, 40, 41]. As the electrophoretic mobility was virtually independent of the NaCl concentration (Fig. 3a), the specifically adsorbed chloride ions are mainly enriched in the interlayer space.

The occurrence of an isoelectric point at 87 mmol/l NaSCN indicates that these anions are strongly adsorbed [1]. The reason of specific adsorption of rhodanide ions is not clear. We note that these ions are the only simple inorganic ions which assemble at the oil/water interface of emulsions [1]. Magnesium aluminum hydroxide could easily be dispersed in paraffin oil [33]. Thus, the surface of the particles probably shows a certain hydrophobic character which promotes adsorption of the rhodanide ions. Because of the strong counterion adsorption, the critical coagulation concentration of NaSCN, 80 mmol/l, approximates the NaSCN concentration at the isoelectric point, 87 mmol/l.

The divalent anions are also strongly adsorbed. The c_K value of Na_2CO_3, Na_2SO_4, and Na_2HPO_4 is, therefore, near the concentration at the point of charge reversal.

The yield value of the dispersions increased continuously up to 80 mmol/l NaCl (Fig. 4a). A shallow minimum as is typical of montmorillonite dispersions [37, 42, 43] could not clearly be detected. Such a minimum at salt concentrations below c_K is caused by the attenuation of the electroviscous effect. This effect is pronounced for particles with high aspect ratios, such as clay mineral particles, and may be too weak for hydroxide particles with axial ratios of 10 or less.

In the presence of divalent counterions the yield value increased steeply at salt concentrations of about 1 mmol/l, corresponding to c_K and the point of charge reversal (Fig. 4b). The liquefying effect of phosphate, which is very pronounced for clay minerals [44], was also observed. The yield value and the viscosity decreased beyond 10 mmol/l Na_2HPO_4. At 100 mmol/l Na_2HPO_4 the yield value was 0.6 Pa in contrast to 5 and 3 Pa at 100 mmol/l Na_2CO_3 and Na_2SO_4.

The increase in the yield stress and the viscosity of the hydroxide dispersions beyond the c_K values of about 1 mmol/l is very likely caused by network formation. Predominant face-to-face aggregation was visualized by freeze-fracture transmission electron microscopy of concentrated dispersions (solid content above 10% w/w) [31]. These dispersions showed unusual rheological behavior. Shaking of freshly prepared dispersions led to an irreversible increase in viscosity. As mentioned previously, antithixotropic behavior, i.e., a reversible increase in viscosity, was observed for the more diluted dispersions.

When the particle charge density increases with the salt concentration as expressed by the mobility curves in the presence of divalent anions (Fig. 3b), the changes of the yield value and the viscosity depend on two opposing effects. As c_K corresponds to the point of charge reversal, the particles aggregate because, owing to the specific adsorption of the divalent anions, the surface charge becomes zero. When the concentration of the divalent anions exceeds c_K, the force between the particles is only weakly attractive if the density of the negative surface charges remains low: the particles form two- or three-dimensional networks. This is the case for sodium carbonate and sulfate. The yield value and the viscosity increase with the salt concentration. In a similar way, phosphate concentrations below 5 mmol/l promote aggregation. At higher concentrations the increased phosphate adsorption raises the surface charge density to a higher value then carbonate and sulfate adsorption (Fig. 3b), and aggregation is reduced.

The question arises why phosphate ions led to a higher mobility and, therefore, to a higher density of negative surface charges than the other divalent anions. The adsorption isotherm showed a plateau of 270 mmol carbonate per mole hydroxide at carbonate concentrations above 60 mmol/l. Phosphate adsorption reached a plateau (160 mmol/mol) at concentrations of 25 mmol/l and greater. If phosphate ions were considered trivalent anions, similar charge equivalents were bound: 540 mEq carbonate and 480 mEq phosphate per mole hydroxide. However, the distribution of these anions between the external surface and the interlayer space may be different. Carbonate ions are preferentially adsorbed in the interlayer space [38]. Thus, a larger part of the phosphate ions is enriched at the external surfaces and increases the negative charge of the particles more strongly than carbonate ions. The mobility of the particles is determined by the charges at the external surfaces; the charges deep in the interlayer space are not important [45, 46].

References

1. Lagaly G, Schulz O, Zimehl R (1997) Dispersionen und Emulsionen. Eine Einführung in die Kolloidik feinverteilter Stoffe einschließlich der Tonminerale. Mit einem historischen Beitrag über Kolloidwissenschaftler von Klaus Beneke. Steinkopff, Darmstadt
2. Lagaly G (1986) In: Wilson AD, Prosser HJ (eds) Developments in ionic polymers, vol 2. Elsevier, London, pp 77–140
3. Jasmund K, Lagaly G (eds) (1993) Tonminerale und Tone. Struktur, Eigenschaften, Anwendung und Einsatz

in Industrie und Umwelt. Steinkopff, Darmstadt
4. Lagaly G (1993) In: Dobias B (ed) Coagulation and flocculation. Theory and applications. Dekker, New York, pp 427–494
5. Lagaly G, Beneke K (1991) Colloid Polym Sci 269:1198–1211
6. Allmann R (1970) Chimia 24:99–108
7. Brindley GW, Kikkawa S (1979) Am Miner 64:836–843
8. Drits VA, Sokolova TN, Sokolova GV, Cherkaskin VI (1987) Clays Clay Miner 35:401–417
9. Marcelin G, Stockhausen NJ, Post JFM, Schutz A (1989) J Phys Chem 93:4646–4650
10. Boehm HP, Steinle I, Vieweger C (1977) Angew Chem 89:259–260
11. Kopka H, Beneke K, Lagaly G (1988) J Colloid Interface Sci 123:427–436
12. Sato T, Fujita H, Endo T, Shimada M, Tsunashima A (1988) React Solids 5:219–228
13. Meyn M, Beneke K, Lagaly G (1990) Inorg Chem 29:5201–5207
14. Dutta PK, Puri M (1989) J Phys Chem 93:376–381
15. Mendibure A, Schöllhorn R (1986) Rev Chim Miner 23:819–827
16. Serna CJ, Rendon JL, Iglesias JE (1982) Clays Clay Miner 30:180–184
17. Thevenot F, Szymanski R (1989) Clays Clay Miner 37:396–402
18. Reichle WT (1985) J Catal 94:547–557
19. Nunan JG, Himelfarb PB, Herman RG, Klier K, Bogdan CE, Simmons GW (1989) Inorg Chem 28:3868–3874
20. Boclair JW, Braterman PS (1998) Chem Mater 10:2050–2052
21. Ribet S, Tichit D, Coq B, Ducourant B, Morato F (1999) J Solid State Chem 142:382–392
22. Olanrewaju J, Newalkar BL, Manicino C, Komarneni S (2000) Mater Lett 45:307–310
23. Dosch W (1965) Zement-Kalk-Gips 18:233–237
24. Dosch W (1967) N Jb Miner Abh 106:200–239
25. Miyata S, Kumura T (1973) Chem Lett 843–848
26. Drezdon MA (1988) Inorg Chem 27:4628–4632
27. Trifiro F, Vaccari A (1996) In: Alberti G, Bein T (eds) Comprehensive supermolecular chemistry, vol 7. Pergamon, Oxford, pp 251–291
28. Newman SP, Jones W (1998) New J Chem 105–115
29. Vaccari A (ed) (1995) Appl Clay Sci 10:1–186
30. Tichit D, Vaccari A (eds) (1998) Appl Clay Sci 13:311–511
31. Albiston L, Franklin KR, Lee E, Smeulders JBAF (1996) J Mater Chem 6:871–877
32. Han S, Wanguo H, Zhang C, Sun D, Huang X, Wang G (1996) J Chem Soc Faraday Trans 94:915–918
33. Abend S, Bonnke N, Gutschner U, Lagaly G (1998) Colloid Polym Sci 276:730–737
34. Schwertfeger M (1996) Thesis. Kiel University
35. Jennings BR (1993) Clay Miner 28:485–494
36. de Rooy N, de Bruyn PL, Overbeek JTG (1980) J Colloid Interface Sci 75:542–554
37. Abend S, Lagaly G (2000) Appl Clay Sci 16:201–227
38. Geismar G, Lewandowski J (1991) Chem-Ztg 115:297–300
39. Lagaly G, Penner D (2000) Clays Clay Miner 48:246–255
40. Lyklema J (1984) J Colloid Interface Sci 99:109–117
41. Lyklema J (1989) Colloids Surf 37:197–204
42. Permien T, Lagaly G (1994) Clay Miner 29:751–760
43. Permien T, Lagaly G (1995) Clays Clay Miner 43:229–236
44. Penner D, Lagaly G (2001) Appl Clay Sci 19:131–142
45. (a) Thomas F, Bottero JY, Cases JM (1989) Colloids Surf A 37:269–280; (b) Thomas F, Bottero JY, Cases JM (1989) Colloids Surf A 37:281–294
46. Thomas F, Schouller E, Bottero JY (1995) Colloids Surf A 95:271–279